



## LJMU Research Online

**Wu, S, Calero-Pérez, P, Villamañan, L, Arias-Ramos, N, Pumarola, M, Ortega Martorell, S, Julià-Sapé, M, Arús, C and Candiota, AP**

**Anti-tumour immune response in GL261 glioblastoma generated by Temozolamide Immune-Enhancing Metronomic Schedule monitored with MRSI-based nosological images**

<http://researchonline.ljmu.ac.uk/id/eprint/11715/>

### Article

**Citation** (please note it is advisable to refer to the publisher's version if you intend to cite from this work)

**Wu, S, Calero-Pérez, P, Villamañan, L, Arias-Ramos, N, Pumarola, M, Ortega Martorell, S, Julià-Sapé, M, Arús, C and Candiota, AP (2020) Anti-tumour immune response in GL261 glioblastoma generated by Temozolamide Immune-Enhancing Metronomic Schedule monitored with MRSI-based**

LJMU has developed **LJMU Research Online** for users to access the research output of the University more effectively. Copyright © and Moral Rights for the papers on this site are retained by the individual authors and/or other copyright owners. Users may download and/or print one copy of any article(s) in LJMU Research Online to facilitate their private study or for non-commercial research. You may not engage in further distribution of the material or use it for any profit-making activities or any commercial gain.

The version presented here may differ from the published version or from the version of the record. Please see the repository URL above for details on accessing the published version and note that access may require a subscription.

For more information please contact [researchonline@ljmu.ac.uk](mailto:researchonline@ljmu.ac.uk)

<http://researchonline.ljmu.ac.uk/>



Supplementary material for:

## ANTI-TUMOUR IMMUNE RESPONSE IN GL261 GLIOBLASTOMA GENERATED BY TEMOZOLAMIDE IMMUNE-ENHANCING METRONOMIC SCHEDULE MONITORED WITH MRSI-BASED NOSOLOGICAL IMAGES

Shuang Wu <sup>[+]</sup>, Pilar Calero Pérez <sup>[+]</sup>, Lucia Villamañan <sup>[+]</sup>, Nuria Arias-Ramos, Martí Pumarola Batlle, Sandra Ortega-Martorell, Margarita Julia Sape, Carles Arús and Ana Paula Candiota

[+] These authors contributed equally to this work.

### SUPPLEMENTARY MATERIALS

#### *MRI studies*

The acquisition parameters were as follows: repetition time (TR)/effective echo time (TE<sub>eff</sub>) = 4200/36 ms; echo train length (ETL) = 8; field of view (FOV) = 19.2 × 19.2 mm; matrix size (MTX) = 256 × 256 (75 × 75 μm/pixel); number of slices (NS) = 10; slice thickness (ST) = 0.5 mm; inter-ST = 0.1 mm; number of averages (NA) = 4; total acquisition time (TAT) = 6 min and 43 s.

#### *MRSI studies*

Consecutive 14 ms echo time (TE) MRSI with point-resolved spectroscopy (PRESS) localization grids were acquired individually across the tumour, using as a reference T2w high resolution images, as described in previous work.<sup>1</sup> First upper (dorsal) grid (Grid 1) had a matrix size of 10 × 10. Then, Grid 2 was acquired 1 mm below Grid 1 with a matrix size of 12 × 12. Grid 3 was acquired 1 mm below Grid 2, also with a matrix size of 12 × 12. Finally, if tumour volume was not completely covered with 3 grids, a final Grid 4 was acquired 1 mm below Grid 3 with a matrix size of 10 × 10.

Acquisition parameters for all grids were: FOV, 17.6 mm × 17.6 mm; VOI in Grids 1 and 4 was 5.5 mm × 5.5 mm × 1.0 mm. VOI in Grids 2 and 3 was 6.6 mm × 6.6 mm × 1.0 mm. ST, 1 mm; TR, 2500 ms; Sweep Width (SW), 4006.41 Hz; NA, 512; TAT, 21 min 30 s each grid. Water suppression was performed with Variable Power and Optimized Relaxation Delay (VAPOR), using a 300 Hz bandwidth. Linear and second order shims were automatically adjusted with Fast Automatic Shimming Technique by Mapping Along Projections (FASTMAP) in a 5.8 mm × 5.8 mm × 5.8 mm volume which contained the VOI region. Six saturation slices (ST, 10 mm; sech-shaped pulses: 1.0 ms/20250 Hz) were positioned around the VOI to minimize outer volume contamination in the signals obtained.

#### *MRSI postprocessing: outline of NMF methods*

In general, NMF methods belong to a group of multivariate data analysis techniques designed to estimate meaningful latent components, also known as sources, from non-negative data. Standard NMF methods decompose a given data matrix “X” into two non-negative matrices: the sources (“S”) and the mixing matrix (“A”). The differences between NMF methods are given by the different cost functions used for measuring the divergence between X and S\*A. A more recent variant of NMF that is also able to handle negative data, namely convex-NMF, was used in this work<sup>2</sup>. Convex-NMF has proven to be able to identify a reduced number of sources that can be confidently recognized as representing brain tumor/tissue types in a way that other source extraction methods, including other NMF variants, cannot detect with the same degree of specificity<sup>3,4</sup>.

### Adapted RECIST criteria

Classification of adapted RECIST criteria was applied as follows: Progressive disease (PD): 20% increase with respect to the smallest tumour volume so far. Partial response (PRE): tumour decrease by 30%, taking into account the biggest volume so far. Stable disease (SDi): less than 20% increase and no more than 30% decrease in tumour volume.

### Protein extraction for WB studies

Whole GL261 tumours obtained after euthanization at endpoint were weighted and 200  $\mu$ L of cold lysis buffer for each 50 mg of tissue was added (cold lysis buffer: 50 mM Tris-HCl pH 7.7, 150 mM NaCl, 15 mM MgCl<sub>2</sub>, 0.4 mM ethylenediaminetetraacetic acid, 0.5 mM dithiothreitol, 100  $\mu$ g/ml of leupeptin, aprotinin and benzamidin and 2 mM of phenylmethanesulfonyl fluoride or phenylmethylsulfonyl fluorid). Samples were homogenized with a 20 G needle 10 times and with a 26 G needle 10 more times. Then, sonication (Fisher Sonic Dismembrator Model 300, Thermo Fisher Scientific, Waltham, MA, USA) was performed five times for 5-s intervals at 30% amplification. After remaining 30 min on ice, the lysate was centrifuged at 13,000 $\times$  g for 20 min at 4  $^{\circ}$ C. Finally, supernatant was collected and used for WB analysis.

### SUPPLEMENTARY FIGURES:

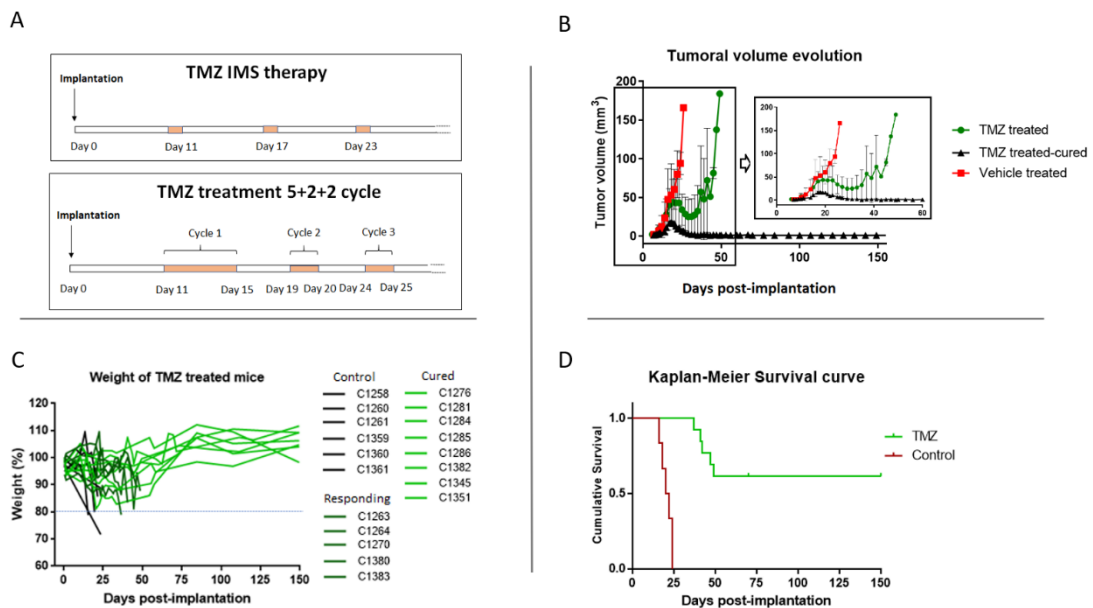


**Figure S1.** (A) Therapeutic schemes for TMZ treatment used in the studies described in this work. First, Immune-Enhancing Metronomic Schedule (IMS) used for GL261 GB therapy in mice- TMZ is administered every six days. Second, TMZ administration schema with 3 therapy cycles with a 3-day interleave, as described previously by us <sup>1</sup>. In both protocols TMZ therapy started at day 11 p.i., except for cases C1100 and C1108, for which the starting day was adapted to tumor volume (see details in supplementary reference 1) (B) Tumour volume evolution for control, vehicle treated (n=6, C1258, C1260, C1261, C1359, C1360 and C1361) and TMZ-treated GL261 tumour-bearing mice with the IMS protocol. For TM-treated mice two groups are shown: responding mice (n=5, cases C1263, C1264, C1270, C1380 and C1383) and cured mice, in which tumour disappeared due to TMZ treatment

(n=8, C1276, C1281, C1284, C1285, C1286, C1345, C1351 and C1382). Mean  $\pm$  SD values are shown. (C) Body weight evolution of GL261 tumour-bearing mice during TMZ treatment with the IMS protocol. Weight is expressed in %, assuming 100% for the weight at day 0; dashed horizontal blue line indicates the 20% weight reduction point, below which animals must be euthanized due to welfare parameters. (D) Kaplan Meier survival comparing GL261 tumour-bearing mice treated with vehicle (n=6) and TMZ (n=13) in an IMS protocol.

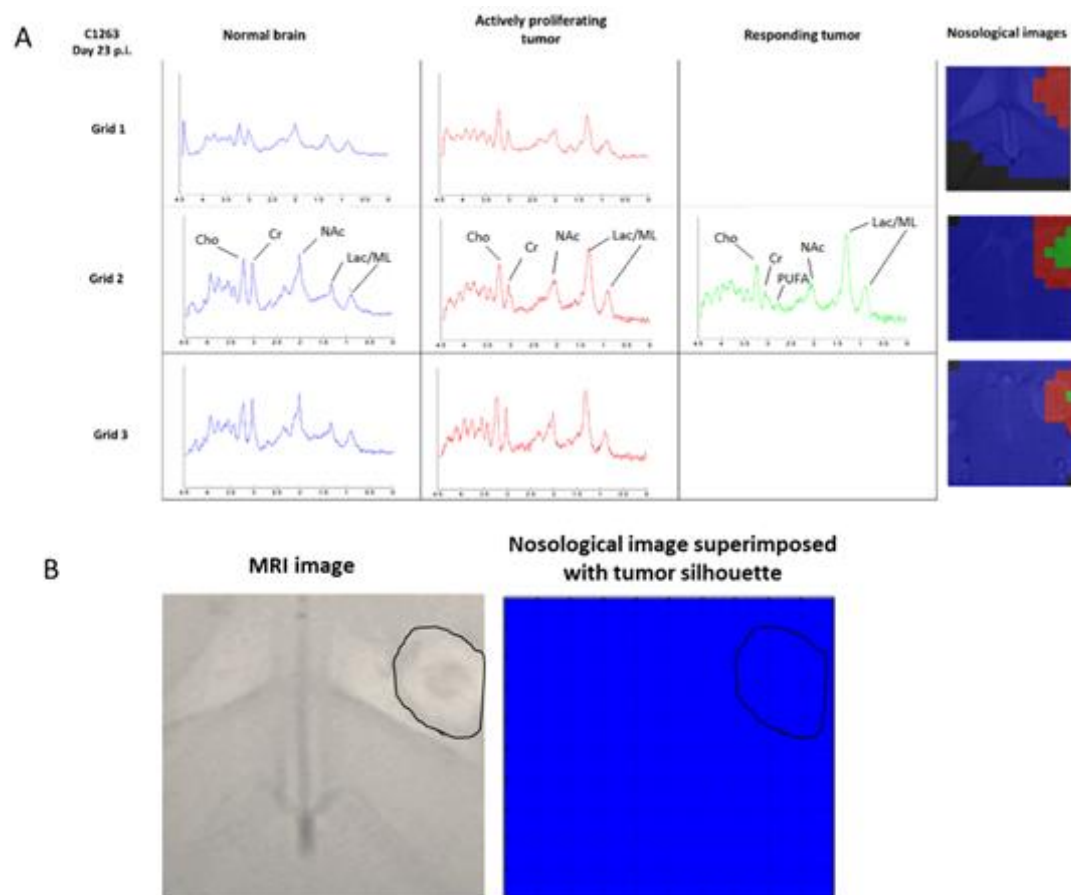


**Figure S2.** (A) Examples of mean spectra calculated from chosen zones of nosological images classified as normal brain parenchyma, actively proliferating tumour and responding tumour in case C1263. Normal brain is shown in blue (n=301 pixels), actively proliferating tumour in red (n=35) and responding tumour in green (n=9). Cho= choline, Cr= creatine, NAc= N-acetyl containing compounds, Lac= lactate, ML= mobile lipids. As expected, tumour zones present higher Cho/Cr and Cho/NAc ratio in comparison with normal brain parenchyma and higher Lac/ML signals. Still, responding zones present more noticeable 2.8 ppm signal, compatible with *Polyunsaturated fatty acids* (PUFA) chemical shift. (B) Example from case 1263 in which the tumour was not recognized by the semisupervised system analysis due to its small size (C1263, day 29 p.i., grid 1) showing one of the handicaps of the technique. In the left side, the MRI image with the tumour mass surrounded in black continuous line. On the right, the nosological imaging mislabeled 'normal' blue over the tumour zone superimposed to the tumour silhouette.

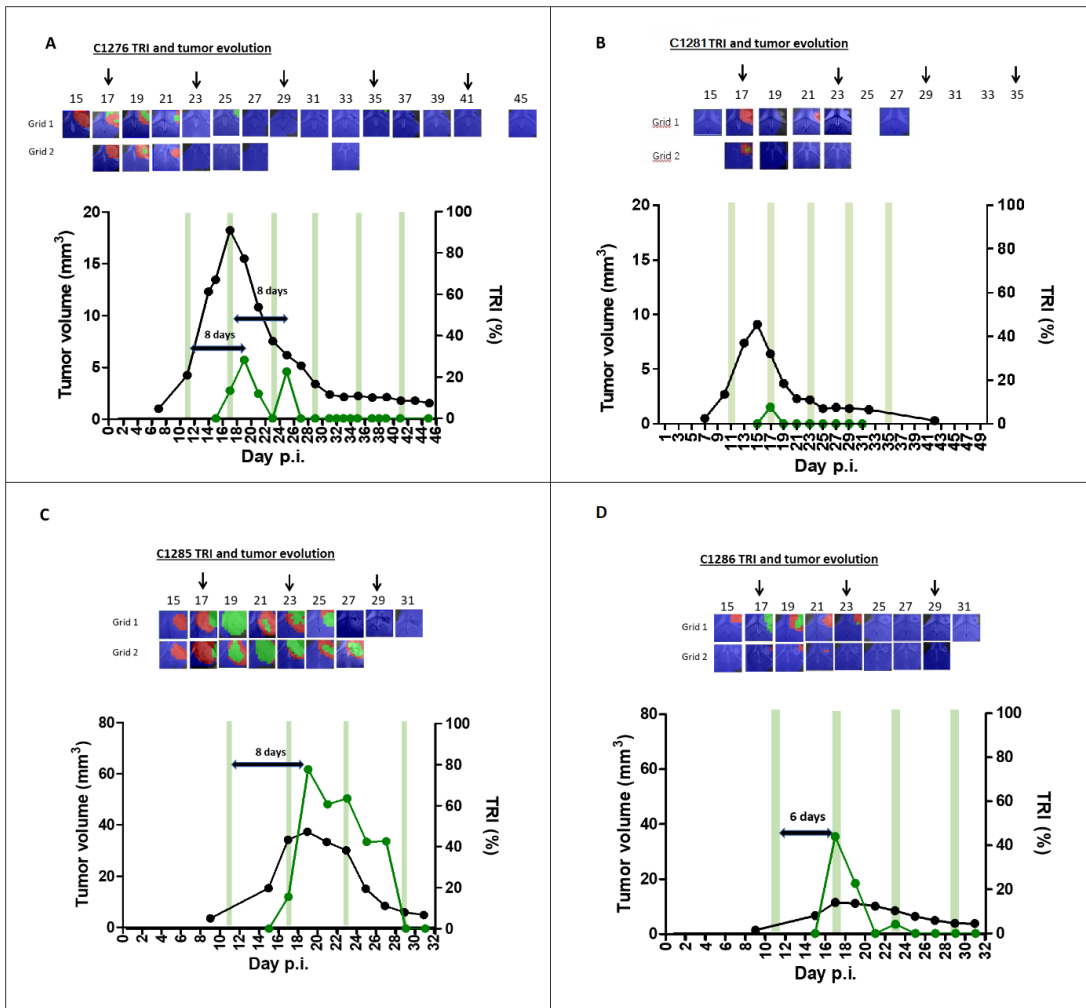


**Figure S3.** Nosological images and graphical representation of the tumour volume evolution for the tumour region in cases (A) C1276, (B) C1281, (C) C1285 and (D) C1286 of “cured” animals. Tumour volume in  $\text{mm}^3$  (black line, left axis) and the percentage of green, responding pixels (TRI) obtained taking into account total pixels counting (green line, right axis). In the upper part of every image chosen time points show the evolution of the nosological images in two rows of color-coded grids superimposed to the T2w-MRI for each slice. Below, green shaded columns indicate TMZ administration days. Case C1284 is not shown because TRI was always below the detection point due to small tumour volume.

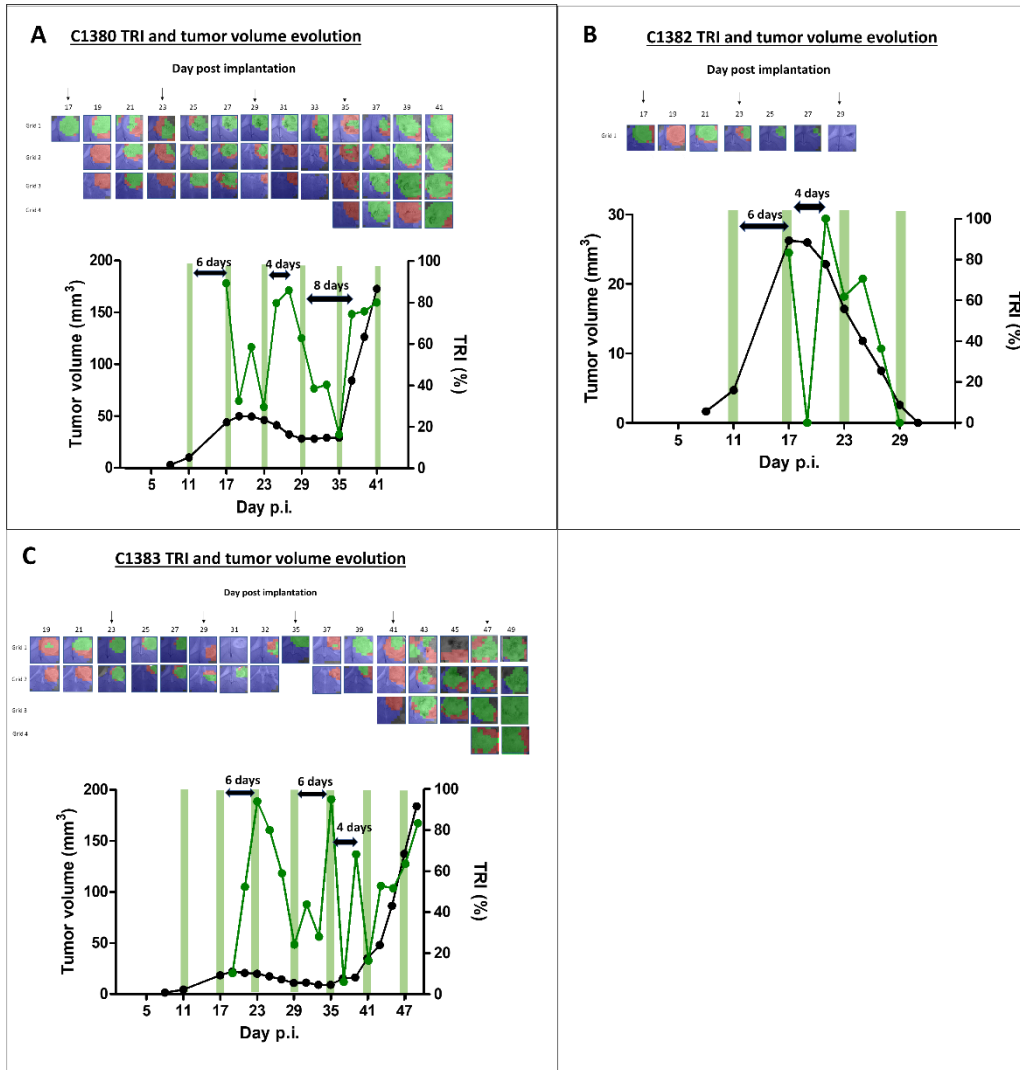


**Figure S4.** Nosological images and graphical representation of the tumour volume evolution for the tumour region in cases (A) C1380, (B) C1382 and (C) C1383. Tumour volume in  $\text{mm}^3$  (black line, left axis) and the percentage of green, responding pixels (TRI) obtained taking into account total pixels counting (green line, right axis). In the upper part of every image chosen time points show the evolution of the nosological images in one to four rows of color-coded grids superimposed to the T2w-MRI for each slice. Below, green shaded columns indicate TMZ administration days.

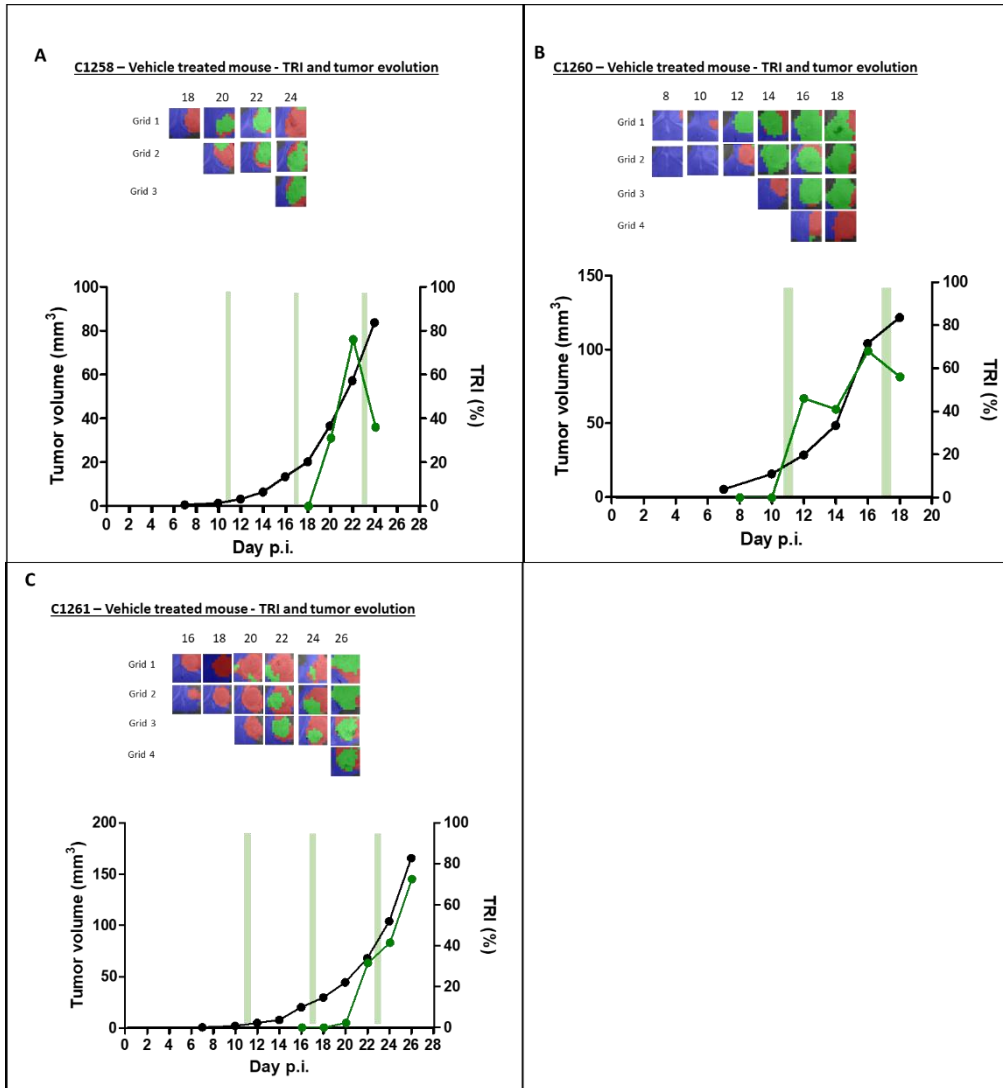


**Figure S5.** Nosological images and graphical representation of the tumour volume evolution for the tumour region in the vehicle treated cases (A) C1258, (B) C1260 and (C) C1261. Tumour volume in mm<sup>3</sup> (black line, left axis) and the percentage of green, responding pixels (TRI) obtained taking into account total pixels counting (green line, right axis). In the upper part of every image chosen time points show the evolution of the nosological images in two rows of color-coded grids superimposed to the T2w-MRI for each slice. Below, green shaded columns indicate TMZ administration days.



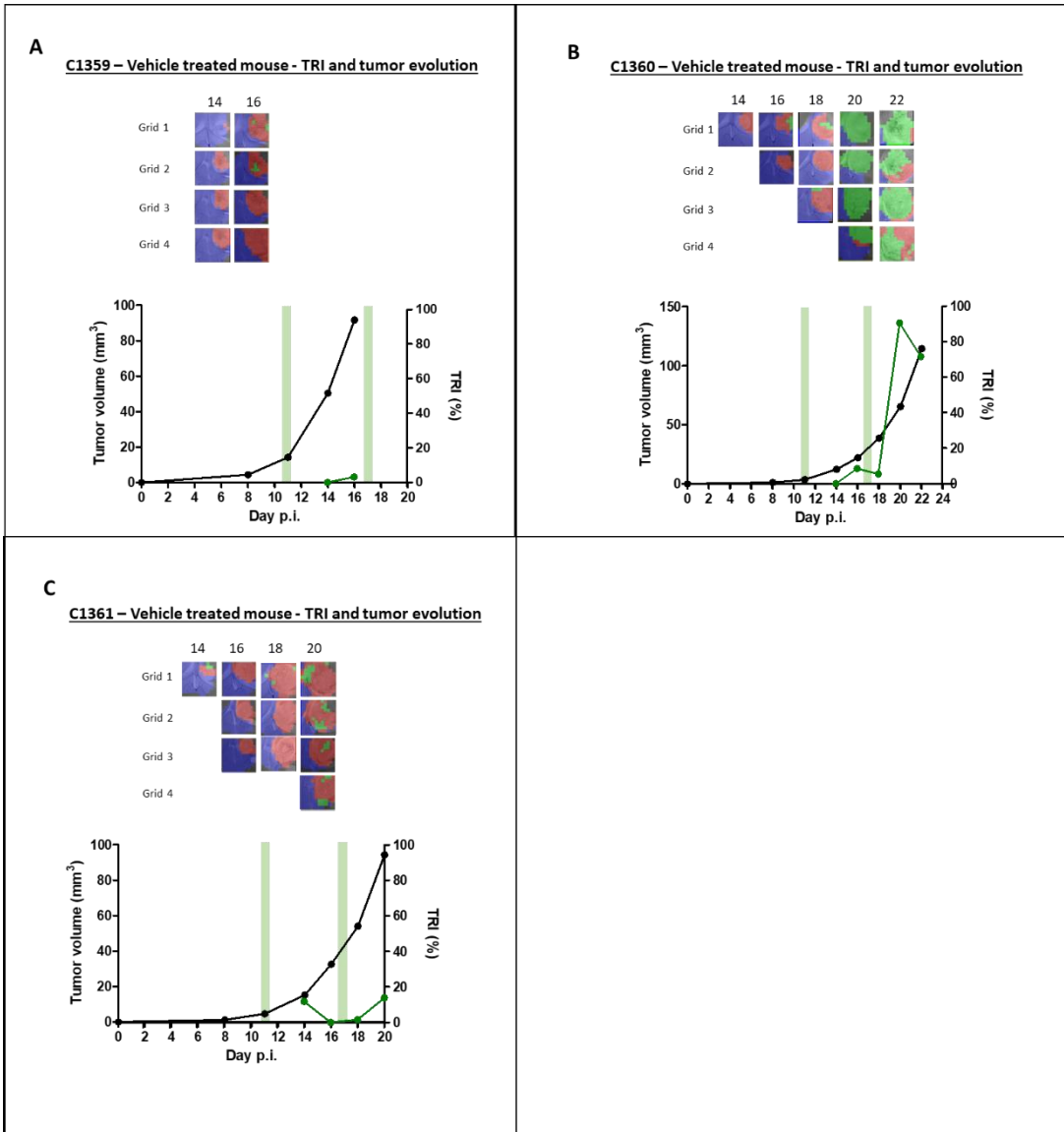


**Figure S6.** Nosological images and graphical representation of the tumour volume evolution for the tumour region in the vehicle treated cases (A) C1359, (B) C1360 and (C) C1361. Tumour volume in mm<sup>3</sup> (black line, left axis) and the percentage of green, responding pixels (TRI) obtained taking into account total pixels counting (green line, right axis). In the upper part of every image chosen time points show the evolution of the nosological images in two rows of color-coded grids superimposed to the T2w-MRI for each slice. Below, green shaded columns indicate TMZ administration days.

## Tumour volume evolution of samples for Western Blot analysis

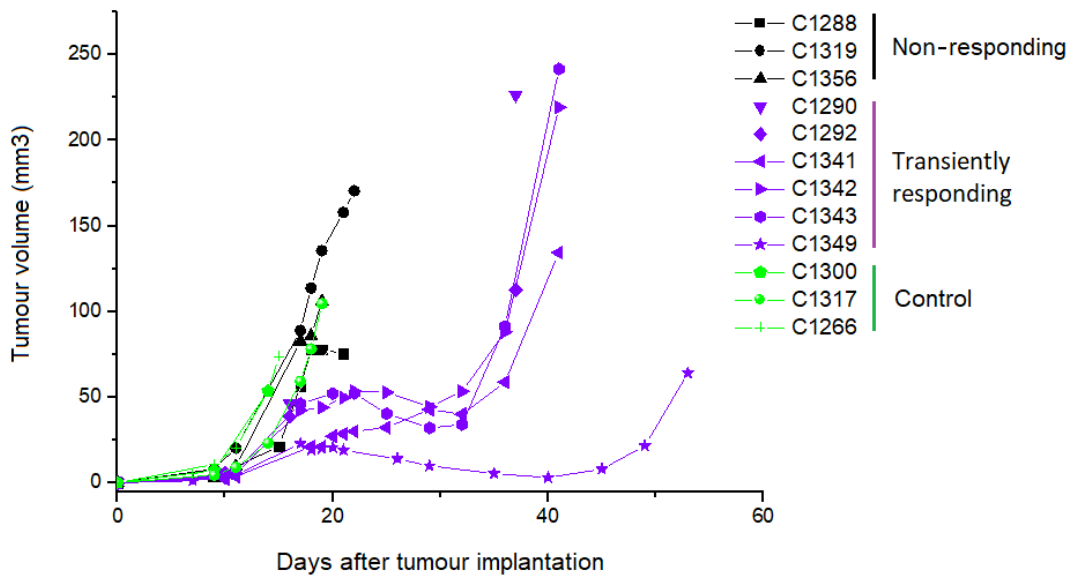


**Figure S7.** Tumour volume evolution for control, vehicle treated (n=3, C1300, C1317 and C1266) and TMZ-treated GL261 tumour-bearing mice with the IMS protocol. For TMZ treated mice two groups are shown: non responding mice (n=3, C1288, C1319 and C1356) and mice showing transient response, in which tumour had transient shrinkage but re-grew after several doses of IMS-TMZ treatment (n=6, C1290, C1292, C1341, C1342, C1343 and C1349). Data for C1290 and C1292 is incomplete (gap from day 16p.i. to day 37p.i.) because of technical issues related to MR scanner time availability in this time period.

## Tumour volume evolution of cured mice

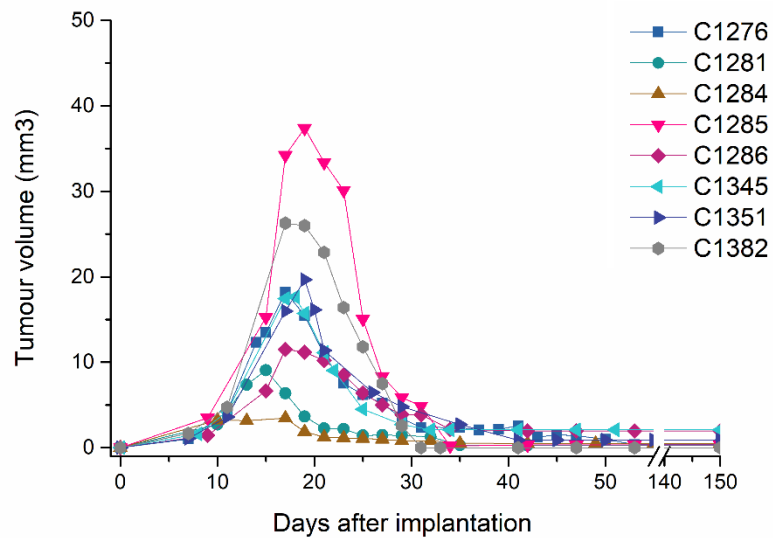


**Figure S8.** Tumour volume evolution of mice cured from TMZ treated group: (n=8, C1276, C1281, C1284, C1285, C1286, C1345, C1351 and C1382).

**SUPPLEMENTARY TABLES:**

**Table S1. Evolution of the TMZ treated GL261 cases considering TRI and tumour volume changes over time.** Classification of adapted RECIST criteria were applied as follows: Progressive disease: 20% increase with respect to the smallest tumour volume so far. Partial response: tumour decrease of 30% taking into account the biggest volume so far. Stable disease: less than 20% of increase and no more of 30% decrease.

<b>Case</b>	<b>Day p.i.</b>	<b>Classification of RECIST criteria</b>	<b>TRI behavior</b>
<b>C1263</b>	17-19	Stable disease	TRI cycles
	21-31	Partial Response	
	33-47	Progressive disease	BDTP and no cycles
<b>C1264</b>	17	Progressive disease	TRI cycles
	19-31	Stable disease	
	33-35	Progressive disease	
	37	Stable disease	No cycles
	39-41	Progressive disease	
<b>C1270</b>	15-19	Progressive disease	TRI cycles
	21-23	Stable disease	
	25-31	Partial Response	
	33	Stable disease	
	35-37	Progressive disease	No cycles
<b>C1276</b>	15-17	Progressive disease	TRI cycles
	19	Stable disease	
	21-27	Partial Response	
<b>C1281</b>	15-17	Stable disease	No cycles
	19-27	Partial Response	
<b>C1284</b>	15-17	Stable disease	No cycles
	19-27	Partial Response	
<b>C1285</b>	15-17	Progressive disease	TRI cycles
	19-23	Stable disease	TRI cycles, then no cycles

	25-31	Partial Response	No cycles
<b>C1286</b>	15-17	Progressive disease	TRI cycles
	19-21	Stable disease	
	23-31	Partial Response	No cycles
<b>C1380</b>	11-17	Progressive disease	TRI cycles
	19-25	Stable disease	
	27-35	Partial Response	
	37-41	Progressive disease	No cycles
<b>C1382</b>	17	Progressive disease	TRI cycles
	19-21	Stable disease	
	23-29	Partial Response	No cycles
<b>C1383</b>	17	Progressive disease	TRI cycles
	19-25	Stable disease	
	27-35	Partial Response	
	37-49	Progressive disease	TRI cycles / No cycles

**Table S2. Evolution of the vehicle-treated cases considering TRI and tumour volume changes over time.**

Classification of adapted RECIST criteria were applied as follows: Progressive disease: 20% increase with respect to the smallest tumour volume so far. Partial response: tumour decrease of 30% taking into account the biggest volume. Stable disease: less than 20% of increase and no more of 30% decrease.

<b>Case</b>	<b>Day p.i.</b>	<b>Classification of RECIST criteria</b>	<b>TRI behavior</b>
<b>C1258</b>	18-24	Progressive disease	One TRI cycle
<b>C1260</b>	8-18	Progressive disease	No cycles
<b>C1261</b>	16-26	Progressive disease	No cycles
<b>C1359</b>	14-16	Progressive disease	No cycles
<b>C1360</b>	14-22	Progressive disease	No cycles
<b>C1361</b>	14-20	Progressive disease	No cycles

**SUPPLEMENTARY REFERENCES:**

1. Arias-Ramos N, Ferrer-Font L, Lope-Piedrafita S, et al. Metabolomics of Therapy Response in Preclinical Glioblastoma: A Multi-Slice MRSI-Based Volumetric Analysis for Noninvasive Assessment of Temozolomide Treatment. *Metabolites*. 2017;7(2):20.
2. Ding C, Li T, Jordan MI. Convex and semi-nonnegative matrix factorizations. *IEEE Trans Pattern Anal Mach Intell*. 2010;32(1):45-55.
3. Ortega-Martorell S, Lisboa PJG, Vellido A, et al. Convex Non-Negative Matrix Factorization for Brain Tumor Delimitation from MRSI Data. Monleon D, ed. *PLoS One*. 2012;7(10):e47824.
4. Ortega-Martorell S, Lisboa PJG, Vellido A, Julia-Sape M, Arus C. Non-negative Matrix Factorisation methods for the spectral decomposition of MRS data from human brain tumours. *BMC Bioinformatics*. 2012;13(1):38.